CHARACTERIZATION METHODS FOR ELASTIC PROPERTIES OF WOOD FIBERS FROM MATS FOR COMPOSITE MATERIALS

R. Cristian Neagu

Ph.D. Student

E. Kristofer Gamstedt

Assistant Professor
KTH Solid Mechanics, Royal Institute of Technology
Osquars backe 1, SE-100 44 Stockholm, Sweden

and

Mikael Lindström

Research Manager
STFI-Packforsk AB, Box 5604
SE-114 86 Stockholm, Sweden

ABSTRACT

Wood fibers offer excellent specific properties at low cost and are of interest as reinforcement in composites. This work compares two alternative test methods to determine the stiffness of wood fibers from simple macroscopic tests on fiber mats. One method is compression of the fiber mat in the thickness direction, which uses a statistical micromechanical model based on first-order beam theory to describe the deformation. The other method is tensile testing of fiber mats and back calculation of the fiber stiffness with a laminate model. Experiments include compression tests and tensile stiffness index tests as well as determination of fiber content, orientation, and dimensional distribution. For mats with unbleached softwood kraft fibers, an effective value of the Young's modulus of 20.1 GPa determined by the compression method can be compared with values of 17.4–19.0 GPa obtained from tensile tests. These are in agreement with values for similar cellulosic fibers found in literature. The compression method is more appropriate for low-density fiber mats, while the tensile test works better for well-consolidated high-density fiber mats. The two methods have different ranges of applicability and are complementary to one another. Limitations of the methods are also discussed. The main advantage of the methods is that they are quantitative. The potential as stiffening reinforcement of various types of fibers can be systematically investigated, even if the fiber mat microstructures are different.

Keywords: Wood fiber, stiffness, fiber mat, test methods, composites.

INTRODUCTION

Background

Wood and cellulose-fiber composites are finding increased use in load-carrying applications since they offer excellent specific properties at a potentially low cost. Wood fibers come from a renewable raw material with almost unlimited availability. They are generally lighter, recyclable, and biodegradable, and they have lower ash content after incineration than, for example, glass fibers. Drawbacks with cellulose-based fibers are their sensitivity to moisture and large variability in properties. The moisture sensitivity derives from the abundance of hydroxyl groups in the cellulosic material (Uesaka 2002). The large variability is explained by differences in fiber structure due to the overall environmental conditions during growth, cambium age, position in tree, and genetic effects (Haygreen and Bowyer 1982).

The largest market share for composite appli-

cations is held by glass fiber-reinforced plastics, and to some extent carbon fiber composites. The wood-fiber composites should first be compared with conventional contending materials like glass mat thermoplastics (GMT) and various sheet molding compounds (SMC). The automotive and building industries are two examples where research and development efforts are being made to use natural fibers as reinforcement in plastics. Automotive applications include door panels, car roofs, package trays, load floors, spare tire covers, etc. In the building sector, typical applications are decking, fencing, railing, windows and doors. Other potential areas of application of wood-fiber composites are in e.g. the packaging and furniture industries. To this end, the mechanical properties and dimensional stability of wood-fiber composites must be better understood.

The main engineering properties of composites to consider at the material selection stage are stiffness, hygroscopic dimensional stability, strength, and fracture toughness. For structural applications with cellulose-based composite materials, the most relevant properties are probably stiffness and hygroscopic dimensional stability. To effectively predict the elastic properties of a composite for a specific application, it is essential to know the elastic properties of the reinforcing fibers. An investigation of the hygroexpansional properties of wood fibers has been presented in a previous paper (Neagu et al. 2005). In this accompanying paper, the stiffness property of wood fibers for composites is focused on.

Methods of stiffness characterization

The increasing market competitiveness demands cost-effective use of materials, as well as more reliable designs. It is therefore enviable, at an early stage in the product development chain, to determine which type of wood fibers has the best potential as reinforcement. The straightforward way to characterize the elastic properties of the fibers is by direct testing of individual fibers. However, single fiber tests are very time-consuming and show daunting variability, meaning that an enormous number of tests must be done to acquire reliable statistics. This is anticipated since the fiber properties vary with e.g. wood species, position in the tree, fiber separation method, etc. (Haygreen and Bowyer 1982; Bergander and Salmén 2000). A more efficient way to determine the elastic properties of the wood fibers would be from simple and convenient macroscopic test methods in combination with an appropriate mechanical model. A common approach is to measure macroscopic composite properties and then use a micromechanical model to back-calculate the fiber properties (Cichocki Jr. and Thomason 2002; Gamstedt et al. 2002; Nordin 2004). Since wood fibers are supplied in the form of sheets, fiber mats, or preforms, it would be desirable to test these semi-manufactured components before the composite is produced. Candidate fiber materials could then be screened at an earlier stage in the processing chain, and the most suitable type of fiber for a certain application could be singled out. Improved cost-effectiveness and a more rational quality control could then be achieved. The aim of this work is to compare alternative test-methods to determine the stiffness of wood fibers from simple macroscopic tests on fiber mats. Two candidate methods are illustrated in the following. Even though these methods have been employed with the aim to select stiff fibers for reinforcement in composite applications, the methods can just as well be used in the context of pulp, paper, and board.

MICROMECHANICAL STIFFNESS MODELS

Two methods of data reduction are considered for the wood fiber mats, namely (1) modeling of the elastic compression in the thickness direction of a fiber assembly with an in-plane fiber orientation distribution and a distribution in fiber cross-sectional dimensions, and (2) use of laminate theory to describe the in-plane elastic behavior of a fiber mat. These are micromechanical models since they use the fiber properties on the microscale to link the microscopic deformation mechanisms to the macroscopic elastic behavior of the fiber mat.

Compression of fiber mats in the thickness direction

The model draws on the seminal work by Toll and Månson (1995), who analyzed the elastic transverse compression of a stochastic planar assembly of fibers, which was subsequently generalized for fibers with a variable cross-section by Alkhagen (2002). These methods are adopted for the specific use in evaluating the wood fiber stiffness in compression of fiber mats. Their applicability is subsequently tested on wood fiber assemblies, where the fiber cross-section shows considerable variability. For completeness, the main features of the compression model proposed by Toll and coworkers are presented in this section with special reference to issues specific for wood fibers.

The distance between fiber contact points will be large in a fiber mat with relatively low density where the fibers are assumed to be long and distributed in one plane with an arbitrary orientation. These are prerequisites for the model proposed by Toll and Månson (1995), which is based on bending of fiber segments between fiber-fiber contact points. The basic idea is that in an assembly of elastic fibers under static compression, the load will be transferred across surfaces of contact between neighboring fibers. A given fiber is thus subjected to a Herzian distribution of contact stresses over its contact surface. If the contact surfaces are small compared to the area of the fiber segment span to the adjacent fiber contact, the surface tractions can be represented as pointwise acting forces. The fiber mat can then be represented by a finite number of contact points interconnected by elastically deformating beams.

In the fiber mat, each fiber makes contact with a number of other fibers crossing above and below, as shown in Fig. 1a. When an external uniaxial pressure is applied, the fibers act as beams supported at the contact points. The segment of the fiber that deflects between two supporting fibers under the load of a third is termed a deforming unit, (cf. Fig. 1b), and can be regarded as a stochastic unit cell (Toll and Månson 1995; Toll 1998). When the network is compressed, more fiber contact points are created and the beam segments that provide resistance to compression become shorter and stiffer. The deforming unit defines also the geometry of the fiber network in a way that resembles the microstructure of the fiber mat. Based on statistical probability methods, essential model parameters such as the number of fiber contacts and the distribution of contact spacing in the fiber mat
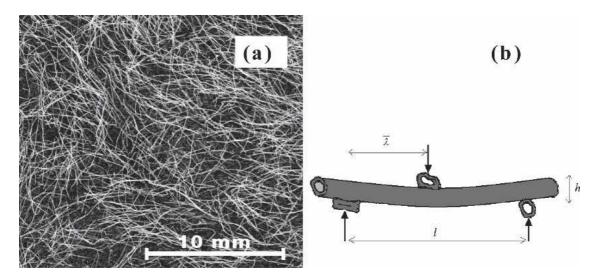

FIG. 1.   (a) Structure of a wood fiber mat. (b) Deforming unit, shown with its characteristic measures: height h and length l which is twice the average contact spacing $\bar{\lambda}$.

can be estimated (Komori and Makishima 1977; Toll 1993; Lu and Carlsson 1996; Alkhagen 2002).

For uniaxial compression, Toll and Månson (1995) derived a relationship between the pressure on the fiber network and the volume fraction of fibers in the network. Upon an increase in the overall external load, it is assumed that the distribution of the incremental forces among all deforming units of a certain height is independent of the deforming unit height. The applied pressure P is related to the volume fraction of the fibers in the fiber mat V_f as

$$P = \int_0^{V_f} \frac{N\langle h \rangle_u^2}{V_f \langle s \rangle_u} \, dV_f \qquad (1)$$

where N is the number of deforming units per unit volume, $\langle h \rangle_u$ is the mean height, and $\langle s \rangle_u$ is the average of the deforming unit compliances, where $\langle \cdot \rangle_u$ denotes average over the number of deforming units. Only elastic reversible deformation is considered. Dissipative mechanisms such as frictional sliding at the contact points and fiber breakage are not taken into account. Strong fiber-fiber bonds imply little or no slip at the beginning of the compression.

It is obvious that the height of a deformation unit h will be proportional to the height of the fibers H. By geometrical considerations under the assumptions of small deformations and low fiber volume fractions, i.e. $h = H$, it can be shown that a small increment in compressive displacement can be expressed as $dV_f/V = -dh/h$. The compliance of a deforming unit can be calculated by using first-order beam theory. If the fiber segment constituting a deformation unit is regarded as a beam loaded at its midsection and fixed at its ends, the average compliance can be expressed as

$$\langle s \rangle_u = \left\langle \frac{1}{192} \frac{l^3}{E_L I} \right\rangle_u = \left\langle \frac{1}{24} \frac{\overline{\lambda}^3}{E_L I} \right\rangle_u \qquad (2)$$

where l, the length of the deforming unit, is substituted with twice the expected contact spacing $\overline{\lambda}$, E_L is the longitudinal Young's modulus of the fibers, and I is the area moment of inertia of the fiber cross-section.

To take the appropriate averages of the parameters in Eqs. (1) and (2), it must be established how the density and distribution of the contact points are related to the fiber volume fraction and the fiber orientation distribution. It should be pointed out that there are many methods that can be used to calculate the number of contact points. See Alkhagen (2002) and Zhu et al. (1995) for a brief outline of some of them. The theory of Toll (1993, 1998) and Alkhagen (2002) is based on probability arguments that can be readily extended to the wood fiber assemblies in this work. It is assumed that the fiber orientation distribution $p(\theta)$ and the fiber height distribution $p(H)$ are mutually independent. It is also assumed that fibers are sufficiently long so that the number of deforming units can be considered equal to the number of contact points. Following the derivation of Alkhagen (2002), the average of any given quantity taken over all contacts is obtained by summation over all contacts divided by the total number of contacts per unit volume

$$\langle \cdot \rangle_c = \frac{V_f}{N \langle A_f \rangle} \langle (\cdot) n_1 \rangle \qquad (3)$$

where A_f is the fiber cross-sectional area and n_1 is the expected number of contacts per unit length of the a fiber with orientation θ and height H, given by

$$\begin{aligned} n_1 &= V_f \langle A_f \rangle^{-1} \langle (H + H')|\sin(\theta - \theta')| \rangle \\ &= V_f \langle A_f \rangle^{-1} (H + \langle H \rangle) \langle |\sin(\theta - \theta')| \rangle \end{aligned} \qquad (4)$$

Equation (4) is obtained by introducing a so-called test fiber with an orientation θ and height H. Then if an arbitrary 'phantom' fiber with orientation θ' and height H' is considered, a unit length of it will intersect a given unit length of the test fiber only if its centerline lies within a volume of size $(H + H')|\sin(\theta - \theta')|$. Setting up the number of intersections of the phantom fibers with the test fiber within a certain orientation-height interval $d\theta' dH'$ and integration over all possible fiber orientations and heights gives the expected number of contacts per unit length of the test fiber n_1 in Eq. (4). Its reciprocal is the expected contact spacing per unit fiber length,

$\bar{\lambda} = n_1^{-1}$. The total number of contacts per unit volume is given in Eq. (5).

$$N = 2V_f^2 \langle A_f \rangle^{-2} \langle\langle |\sin(\theta - \theta')| \rangle\rangle \qquad (5)$$

where the double average is defined as

$$\langle\langle \cdot \rangle\rangle = \iiiint (\cdot)p(\theta)p(\theta')p(H)p(H')\mathrm{d}\theta\mathrm{d}\theta'\mathrm{d}H\mathrm{d}H' \qquad (6)$$

Substituting Eqs. (4) and (5) into Eq. (3), the average over the contact points can be rewritten as

$$\langle \cdot \rangle_c = \frac{\langle\langle (\cdot)(H + H')|\sin(\theta - \theta')| \rangle\rangle}{2\langle H \rangle f} \qquad (7)$$

where f is an invariant of the fiber distribution orientation defined as (Toll 1993)

$$f = \langle\langle |\sin(\theta - \theta')| \rangle\rangle = \iint |\sin(\theta - \theta')| p(\theta)p(\theta')\mathrm{d}\theta\mathrm{d}\theta' \qquad (8)$$

The fiber orientation distribution function $p(\theta)$ can be represented as a normalized Fourier series expansion of the probability density function

$$p(\theta) = \frac{1}{\pi} \sum_{n=0}^{\infty} a_n \cos(2n\theta) \qquad (9)$$

with $a_0 = 1$ and the rest of an arbitrary number of Fourier cosine coefficients a_n can be determined experimentally. The angle θ is the direction for a fiber relative to a predetermined direction, typically the machine direction (MD). Using Eq. (9) with the definition of f in Eq. (8), a closed form expression can be obtained as

$$f = \frac{2}{\pi} - \sum_{n=0}^{\infty} \frac{a_n^2}{4n^2 - 1} \qquad (10)$$

which takes values from 0 for a unidirectional to $2/\pi$ for a uniform fiber orientation distribution.

Assuming that the contact points along a given fiber are randomly spaced, the third moment of the expected contact spacing in Eq. (2) can be evaluated as $\bar{\lambda}^3 = 6\lambda^3$. Then the contact spacing in Eq. (2) can be substituted with its reciprocal, which is the inverse of the expected number of contacts per unit length of the fiber, n_1 in Eq. (4). Finally Eq. (7) is applied to Eqs. (1)

and (2), which after integration with Eq. (5) results in

$$P = \frac{2\langle A_f \rangle^{-5}(\langle H^2 \rangle + \langle H \rangle^2)^2 f^4}{5\langle I^{-1}(H + \langle H \rangle)^{-2} \rangle} E_L V_f^5 \qquad (11)$$

The effects of fiber orientation distribution, fiber segment loading, boundary conditions, and variability in fiber cross-sectional dimensions enter the above relationship as a direct proportionality factor to the fiber stiffness times the volume fraction of fibers raised to the power of 5, i.e. $P = CE_L V_f^5$.

The fiber dimensions and their variation are important model parameters and must be determined. For a rational characterization of the cross-sectional dimension of the fibers, image analysis methods and software are today widely available. However, the majority of these programs have been developed for stereological investigations for application in the field of metallurgy, histology, etc. In the pulp and paper research community, image analysis software is typically used to determine the fraction of latewood (thick-walled boxlike) and earlywood (collapsed) fibers from micrographs of a paper sheet cross-section together with their corresponding geometric parameters (Reme et al. 1999). Image analysis software can be used to determine geometric parameters such as the cross-sectional areas, perimeter, etc. from micrographs of a fiber mat cross-section as illustrated in Fig. 2a. Quantities like the area moment of inertia are usually not included in these softwares. It is therefore necessary to estimate the area moment of inertia from the typically quantified values: fiber area A_f, maximal fiber height H, maximal fiber width W, lumen area A_{lu}, maximal lumen height H_{lu}, and maximal lumen width W_{lu} as shown in Fig. 2b. Treating the cross-section as boxed shape would significantly overestimate the area moment of inertia. It would therefore be better to use the measured quantities and fit a superellipse with the general formula $|y/a|^r + |z/b|^r = 1$ to represent the fiber cross-section. The parameters a and b are given by half the fiber/lumen width and height, respectively, as indicated in Fig. 2b. The parameter r is
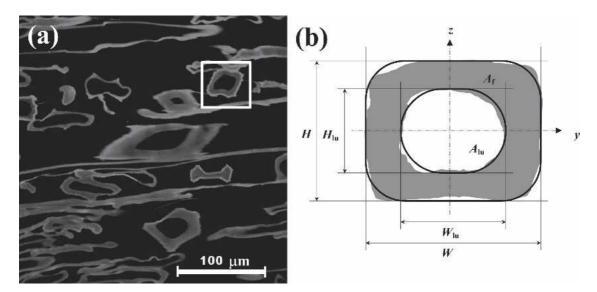
FIG. 2.   (a) Confocal microscopy image of fiber cross-sections. (b) Fiber geometric parameters used to fit a superellipse to the fiber cross-section.

obtained by fitting the measured fiber/lumen areas to

$$A = abrB\left(\frac{r}{2}, \frac{r}{2}\right) \qquad (12)$$

where B denotes the beta function. The area moment of inertia can then be calculated with (Jaklic and Solina 2003)

$$I = \frac{1}{2} ab^3 rB\left(\frac{3r}{2}, \frac{r}{2}\right) \qquad (13)$$

The volume fraction of fibers V_f of the mat can be determined with respect to the applied pressure P from load-displacement data of compression tests of fiber mats if fiber mat grammage, initial thickness, and cell-wall density are known. The fiber orientation distribution and the fiber cross-sectional dimensions are also necessary input parameters since they determine the proportionality factor in the power law relation given by Eq. (11). The fiber stiffness can subsequently be determined from the intercept of the straight line of slope 5 if the power relation is represented in double logarithmic scale. If dealing with large experimental series, it might be valuable to utilize a statistical data reduction step as described in the next section. A con-

densed database with geometric distribution parameters for many fiber types could then be established.

Statistical data reduction

For efficient data processing, it is of interest to use statistical inference to formulate a probability distribution that describes the variability of a population as accurately as possible. A lognormal distribution can be used to represent the variation in wood fiber cross-sectional dimensions. This distribution has become an important measurement model in engineering sciences as an alternative to normal Gaussian distribution, since its sample space admits only positive values and its shape more naturally fits many measured data frequency patterns. The lognormal distribution is frequently used for strength and lifetime data. A continuous random variable X has a lognormal distribution if its probability density function has the form

$$f_X(x) = \frac{1}{x\sigma\sqrt{2\pi}} \exp\left(-\frac{1}{2}\left(\frac{\ln x - \mu}{\sigma}\right)^2\right)$$
$$(14)$$

where two parameters, the mean logarithm value μ, and the standard deviation σ, suffice to de-

scribe large sample data. The lognormal distribution also shows considerable flexibility of shape, but is however always skewed to the left with a longer right tail. Moreover, because of its close relation to the normal distribution, many of the exact normal inferential procedures transfer directly to the lognormal distribution (Bury 1998).

The distribution parameters that describe the variability of the fiber height H, area A_f, and area moment of inertia I are easily obtained as the maximum likelihood estimates. Then the total sample averages that enter Eq. (11) can be replaced with the expectation of the function that describes the random variable. Thus, once the distribution parameters are known, Eq. (11) can be rewritten in terms of the expectations, denoted E[·], and variance, denoted Var[·], as

$$P = \frac{E[A_f]^{-5}(2E[H]^2 + Var[H])^2}{(E[I^{-1}]E[(H + E[H])^{-2}]}\frac{2}{5}f^4 E_L V_f^5 \quad (15)$$
$$+ Cov[I^{-1},(H + E[H])^{-2}])$$

where $Cov[I^{-1},(H + E[H])^{-2}]$ is the covariance given by the interdependence between I^{-1} and $(H + E[H])^{-2}$, which must be determined numerically directly from the sample data. Moments of a random variable give useful measures that characterize the chosen statistical model. The nth moment about the origin of a random variable X with a lognormal distribution is

$$\mu_n'(X) = \exp\left(n\mu + \frac{n^2\sigma^2}{2}\right) \quad (16)$$

For $n = 1$ the expected value of X results: $E[X] = \mu_1'$ gives the average value of all possible measurements on X. The mean of the inverse of X, $E[X^{-1}]$, is obtained by substituting $n = -1$ in Eq. (16). Hence closed form algebraic expressions can be obtained for expected values of powers of H, A_f, and I^{-1} as functions of their respective distribution parameters. The variance of X given in Eq. (17) is defined as the second moment of X about the mean $E[X]$:

$$Var[X] = \exp(2\mu + \sigma^2)(\exp(\sigma^2) - 1) \quad (17)$$

The variance is a measure of the spread and its square root gives the standard deviation as the spread in the units of measurements. To evaluate the term $E[(H + E[H])^{-2}]$ in the denominator of Eq. (15), the definition of the expectation results in an improper integral that cannot be expressed explicitly in a closed form. An improved approach to compute the integral is to rewrite the expected value and replace the infinite limit with a finite value. This will certainly also facilitate the numerical integration procedure. For this reason, the sought-expected value $E[(H + E[H])^{-2}]$ can be computed from the distribution of a continuous random variable Y defined as

$$Y = \frac{1}{(H + \mu_1'(H))^2} \quad (18)$$

where $H = \exp(Z)$ and Z is a continuous random variable normally distributed with expected value μ and standard deviation σ. Since H takes values from zero to infinity, the possible values of Y are given by the interval 0 to $1/(\mu_1'(H))^2$. For t on the interval, the cumulative distribution function of Y is readily obtained using the variable substitution in Eq. (18) as

$$F_Y(t) = 1 - F_Z\left(\log\left(\frac{1}{\sqrt{t}} - \mu_1'(H)\right)\right) \quad (19)$$

where $F_Z(\cdot)$ is the normal cumulative distribution function. The density function of Y can be obtained in terms of $f_Z(\cdot)$ by taking the derivate of Eq. (19) with respect to t. The expected value of Y can then be calculated from the integral

$$E[Y] = E\left[\frac{1}{(H + \mu_1'(H))^2}\right]$$
$$= \int_0^{1/(\mu_1'(H))^2} \frac{1}{2(1 - \mu_1'(H)\sqrt{t})}$$
$$f_z\left(\log\left(\frac{1}{\sqrt{t}} - \mu_1'(H)\right)\right)dt \quad (20)$$

Now Eqs. (16), (17), and Eq. (20) can be inserted into Eq. (15) to give a direct proportionality factor to $2fE_L V_f^5/5$ expressed in terms of the distribution parameters of the fiber cross-

sectional dimensions. The advantage of using this statistical data reduction step is that the large amount of data obtained from the image analysis of the fiber mat cross-section can be condensed to merely a few parameters that describe the dimensional variability. Once the proportionality factor has been determined for a specific fiber type, the experimental evaluation procedure is facilitated in analysis of mats with the same kind of fiber but with different density and fiber orientation.

Tensile stiffness index of fiber mats

The model outlined above is applicable on fiber mats with low density and long fibers. For fiber mats of fairly high density with strong bonds and long fibers, laminate theory can be used to model their in-plane elastic behavior. The fiber mat can be considered as a homogeneous lamina where an orthotropic constitutive relation describes its in-plane properties (Schulgasser and Page 1988; Neagu et al. 2005). The principal directions of the laminate coincide with the direction of manufacture (MD) and the perpendicular cross direction (CD). The elastic properties of wood fibers are highly anisotropic, and the stiffness parameters depend primarily on the fibril angle in the S_2 layer of the cell wall (Page et al. 1971; Page et al. 1977). The helical structure of the fiber implies that axial deformation is coupled with torsion. Taking this coupling into account would require a very detailed analysis, which is not pertinent to the present investigation. Instead, the fibers are assumed to be transversely isotropic and uniform, which overlooks the extension-twist interaction and the presence of lumen. For high-density sheets, the lumen is generally collapsed, even for most latewood fibers, due to high nip pressure at the consolidation state.

The elastic behavior of an individual fiber embedded in the fiber mat is based on the assumptions outlined by Schulgasser and Page (1988). It is reasonable to assume that (1) the fibers lie in the plane of the fiber mat and are constrained from rotating out of the plane, (2) there are few

if any unbonded fiber segments whose lengths are comparable with or larger than the fiber width, (3) each fiber is sufficiently bonded so that the influence of the ineffective length of shear load transfer at the fiber end is negligible, and (4) uniform in-plane strain throughout all material and absence of any out-of-plane stresses are assumed. The laminate model should apply to well-bonded fiber mats while network models (Cox 1952) can be used to predict the elastic response of lightly bonded low-density mats. These two models represent bounds of fiber mat behavior, with the actual response lying between the two extremes since in reality there are variations in the local strain in fiber mat under load. As a consequence for medium-density fiber mats, a mosaic model that accounts for differences in stiffness in bonded and unbonded regions would provide a more accurate description (Lu et al. 1995; Lu et al. 1996).

The components of the fiber stiffness matrix are related to the engineering constants as $Q_{11} = E_L/(1 - \nu_{LT}\nu_{TL})$, $Q_{22} = E_T/(1 - \nu_{LT}\nu_{TL})$, $Q_{12} = \nu_{LT}E_T/(1 - \nu_{LT}\nu_{TL})$ and $Q_{66} = G_{LT}$. To account for the inherent porosity of the fibers and of the fiber mat, the stiffness matrix of fiber should be multiplied with the volume fraction of fibers in the fiber mat.

The effective stiffness matrix of a fiber mat with a non-uniform fiber orientation distribution $p(\theta)$ given by Eq. (9) can be obtained through a laminate analogy. Using invariant properties and lamination parameters (Tsai and Hahn 1980), a closed-form formulation can be developed for the Young's moduli of the orthotropic fiber mat, E_{MD} and E_{CD}, as a function of the unknown engineering elastic constants of the fibers, viz. E_L, E_T, ν_{LT} and G_{LT}. To reduce the number of unknowns, one can impose certain reasonable relations between these values by comparing different reported data in the literature. Let $R_A = E_L/E_T$ and $R_S = G_{LT}/E_L$ denote the anisotropy ratio and the ratio of shear to the longitudinal elastic modulus, respectively. If the major Poisson ratio is known, then E_L can be determined by minimizing the least square sum of the ex-

perimentally measured values which gives the following expression

$$E = \frac{\rho_f(R_A - v_{LT}^2)\left(E_{MD}^{exp}\dfrac{\partial E_{MD}}{\partial E_L} + E_{CD}^{exp}\dfrac{\partial E_{CD}}{\partial E_L}\right)}{\rho(f_{11}f_{22} - f_{12}^2)\left(f_{22}^{-1}\dfrac{\partial E_{MD}}{\partial E_L} + f_{11}^{-1}\dfrac{\partial E_{CD}}{\partial E_L}\right)}$$

(21)

where E_{MD}^{exp} and E_{CD}^{exp} are the measured Young's moduli of the fiber mat in MD and CD, respectively, ρ is the density of the fiber mat, and ρ_f the density of the fibers, and f_{11}, f_{22} and f_{12} are functions that include the effect of anisotropy and fiber orientation and can be expressed

$$f_{11} = \frac{1}{4}a_1(R_A - 1) + \left(1 - \frac{a_2}{2}\right)$$
$$\left[\frac{v_{LT}}{4} + \frac{R_S}{2}(R_A - v_{LT}^2)\right] + \frac{1 + R_A}{8}\left(3 + \frac{a_2}{2}\right)$$

$$f_{22} = \frac{1}{4}a_1(1 - R_A) + \left(1 - \frac{a_2}{2}\right)$$
$$\left[\frac{v_{LT}}{4} + \frac{R_S}{2}(R_A - v_{LT}^2)\right] + \frac{1 + R_A}{8}\left(3 + \frac{a_2}{2}\right)$$

$$f_{12} = \frac{v_{LT}}{4}\left(3 + \frac{a_2}{2}\right) + \left(1 - \frac{a_2}{2}\right)$$
$$\left[\frac{1 + R_A}{8} - \frac{R_S}{2}(R_A - v_{LT}^2)\right]$$

(22)

where a_1 and a_2 are Fourier cosine coefficients of the distribution function given in Eq. (9). Expressions for the Young's moduli of the fiber mat E_{MD} and E_{CD}, obtained from the inverse of the fiber mat stiffness matrix, are differentiated with respect to E_L. The derivate of E_{MD} can be evaluated as

$$\frac{\partial E_{MD}}{\partial E_L} =$$
$$\frac{\rho}{\rho_f(R_A - v_{LT}^2)}\left[\left(1 - \frac{R_A}{R_A - v_{LT}^2}\right)\left(f_{11} - \frac{f_{12}^2}{f_{22}}\right)\right.$$
$$\left. + E_L\left(\frac{\partial f_{11}}{\partial E_L} - \frac{f_{12}}{f_{22}}\left(2\frac{\partial f_{12}}{\partial E_L} - \frac{f_{12}}{f_{22}}\frac{\partial f_{22}}{\partial E_L}\right)\right)\right]$$

(23)

of E_{CD} as

$$\frac{\partial E_{CD}}{\partial E_L} =$$
$$\frac{\rho}{\rho_f(R_A - v_{LT}^2)}\left[\left(1 - \frac{R_A}{R_A - v_{LT}^2}\right)\left(f_{22} - \frac{f_{12}^2}{f_{11}}\right)\right.$$
$$\left. + E_L\left(\frac{\partial f_{22}}{\partial E_L} - \frac{f_{12}}{f_{11}}\left(2\frac{\partial f_{12}}{\partial E_L} - \frac{f_{12}}{f_{11}}\frac{\partial f_{11}}{\partial E_L}\right)\right)\right]$$

(24)

The partial derivates of the f_{11}, f_{12}, and f_{22} functions can be obtained by derivation of the expressions given in Eq. (22). The longitudinal fiber elastic modulus in Eq. (21) can now be solved using Eqs. (22)–(24). The fiber anisotropy ratio, shear to longitudinal elastic modulus ratio, fiber major Poisson ratio, and of course the measured fiber mat elastic moduli must be known.

EXPERIMENTAL PROCEDURES

Materials and specimen manufacture

Unbleached softwood kraft fibers were used. Hand-chipped and screened Norway spruce was cooked and processed according to conventional procedures to a kappa number of 46. Fiber mats with a random in-plane fiber orientation distribution were prepared in form of handsheets manufactured according to standard ISO 5269–1:1998. Oriented fiber mats were also prepared from the same pulp batch using a dynamic sheet former. Detailed process procedures are given in Neagu et al. (2005). Different orientation distributions were used to illustrate the generality of the methods with respect to fiber orientation. Four quadratic specimens with a side length of 50 mm were cut out from the isotopic fiber mat for compressive testing. One specimen was subsequently used to confirm that the orientation distribution of the handsheet was indeed uniform. From the oriented fiber mats, specimens were made for tensile testing with dimensions of 100 mm × 15 mm cut both along the MD and the CD.

Determination of fiber content, orientation, and cross-section

The grammage was determined according to standard ISO 536:1995. To define the density, the structural thickness of the fiber mats was measured with two surface profilometers on opposite sides of a nip through which the specimens were pulled (Fellers et al. 1986). The apparatus was carefully calibrated with a reference thickness, from which a deviation is measured.

The fiber orientation distribution was determined by a tape-splitting technique (Neagu et al. 2005). Two individual layers, the topside and the wireside, were analyzed. The successive splitting procedure was pursued until the sublayers contained an appropriate grammage for image analysis. Image analysis software, which uses gradient analysis by edge detection, was employed to determine the fiber orientation distribution. The results are classified in histograms with relative number of fibers in each angle interval with respect to the MD.

To determine the cross-section geometry of the fibers, confocal laser scanning microscopy was used. The principles for and examples of several applications of this technique to pulp and paper research are given by Moss et al. (1993). Micrographs, illustrated in Fig. 2a, were taken representatively and uniformly over the cross-section. A total number of 40 pictures were taken on each sample. The micrographs were analyzed with the commercial image analysis program Optimate 6.2 (Media Cybernetics). A suitable threshold was empirically determined so that the thresholded images would have the best resemblance with the observed contours of the fibers in the original images. Manual manipulation of every image was done in order to separate fibers of interest from artefacts. When the images had been edited, the program calculated the fiber dimensions. Only fibers lying almost perpendicularly to the plane of the specimens were analyzed. Cross-sectional parameters were obtained as the maximum and minimum fiber height and width, maximum and minimum lumen height and width, fiber cell-wall area and thickness, lumen area, fiber and lumen perimeters.

Compressive and tensile testing of the fiber mats

An MTS testing machine with a load cell of 40 kN in load control was used for compressive testing. Two parallel plates were pressed together with the fiber-mat specimen in between them while the load and displacement were recorded, as shown in Fig. 3. The specimens were compressed to a load of 1 kN in 0.5 s and unloaded at the same rate. The distance between the press platens was measured as the mean value of the signals from two eddy current transducers (Kaman Multi-Vit) at a sampling rate of 100 Hz. The fiber volume fraction V_f could be determined directly from the distance between the press platens since the grammage and cell-wall density were known. For each specimen, the relationship between the pressure and the fiber volume fraction during the on-loading part was used to describe the compaction behavior of the isotropic fiber mat.

The tensile stiffness index, equivalent to the Young's modulus divided by the fiber mat density, was measured according to standard SCAN-P 67:93, using a paper tensile tester from Lorentzen & Wettre AB. All experiments were performed at room temperature 23°C and relative humidity of 50%.
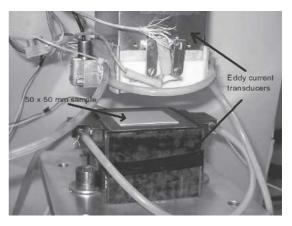

FIG. 3. Experimental set-up for compressive testing of the fiber mats.

RESULTS AND DISCUSSION

The results of the microstructural characterization are presented before the models are employed to estimate the effective Young's modulus of the fibers. Finally the two methods are compared and advantages and disadvantages are outlined.

For the isotropic and oriented fiber mats, the grammage was determined to 185 g/m^2 and 187 g/m^2, respectively. The thickness measurements resulted in an initial thickness of 0.616 mm for the isotropic fiber mat and a thickness of 0.557 mm for the oriented fiber mat. This implies that the isotropic fiber mat had an initial density of 300 kg/m^3, which is slightly lower than the density of the oriented fiber mat of 336 kg/m^3.

Fiber orientation measurements on the isotropic fiber mat confirmed that the fiber orientation distribution was virtually uniform. Results obtained for the wireside and topside of the fiber mat shown in Fig. 4a demonstrate a near-uniform distribution. The Fourier cosine coefficients of the distribution function of the fiber orientation distribution a_1 and a_2 can be assumed to be zero for isotropic fiber mats.

The through-thickness variation of the orientation distribution of the oriented fiber mat has been presented by Neagu et al. (2005). It was concluded that fiber mats manufactured with the dynamic sheet former have a fiber orientation distribution that is symmetric with respect to the MD throughout the thickness of the sheet and has a thickness gradient, which is evidence of a non-negligible two-sidedness. In Fig. 4b the measured orientation distribution histogram with a corresponding fit to the orientation distribution function given by Eq. (9) is shown for the wire and topside of the oriented fiber mat. For the purpose of this work, average values for the orientation parameters, $a_1 = 1.26$ and $a_2 = 0.62$, suffice to account for the influence of the fiber orientation. The fact that the fiber mat has a thickness gradient of fiber orientation can be exploited to estimate the hygroexpansion coefficient of the fibers (Neagu et al. 2005).

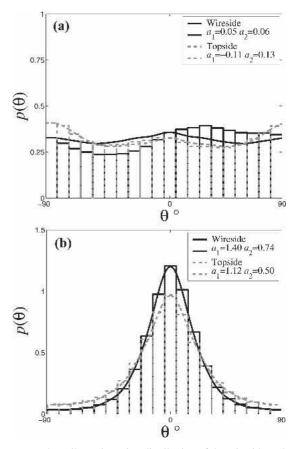To obtain the necessary geometric parameters of the fiber cross-section, a total of 215 fibers

FIG. 4. Fiber orientation distribution of the wireside and topside of (a) the isotropic fiber mat and (b) the oriented fiber mat.

were analyzed. This number should be representative for the whole fiber population in the fiber mat. A lognormal distribution was used to represent the distribution of wood fiber cross-sectional dimensions. The results are summarized in Table 1 as estimated lognormal distribution parameters, μ (mean of logarithm value) and σ (corresponding standard deviation) of the geometric parameters: fiber height H, fiber width W (see Fig. 2b), cross-sectional fiber area

TABLE 1. *Lognormal distribution parameters of fiber geometries.*

Parameter	H (μm)	W (μm)	A_f (μm^2)	I (10^3μm^4)
Mean value μ	2.44	3.84	5.93	8.46
Standard deviation σ	0.74	0.39	0.50	1.95

A_f and the calculated area moment of inertia I. Kolmogorov-Smirnov goodness-of-fit tests were performed to verify that the cross-section dimensions follow a lognormal distribution at a significance level of 5%. The Kolmogorov-Smirnov statistic also showed that the lognormal distribution is generally a better candidate than the two-parameter Weibull distribution for the measured dimensions.

Compression test results

Compression test results for one of the specimens are shown in Fig. 5. The density of the fiber wall ρ_f can be assumed to be 1500 kg/m^3 (Kajanto et al. 1998). The density of the fibers was estimated as ρ_f times a correction factor to include the lumen with unchanged volume, since the deformation mechanism is assumed to be beam bending where no transverse compression of the cell-wall is allowed. A correction factor of 0.77 was calculated as the average of the ratios of fiber wall area to total fiber area including the lumen in cross-section images.

An effective value of the longitudinal Young's modulus of the fibers can be obtained by fitting the power law expression given in Eq.
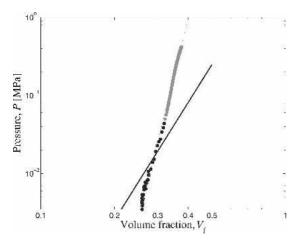

FIG. 5.   Double logarithmic plot of pressure vs. volume fraction from a compression test. Gray squares represent all experimental data to which an arbitrary power law function is fitted, i.e. the dashed line. The black continuous line is a linear regression of Eq. (11) to truncated experimental data only, given by the black circles.

(11) to the experimental data in Fig. 5. Fitting of an arbitrary power law function (dashed-dotted gray line in Fig. 5) resulted in an exponent higher than the expected exponent of five. The fix exponent value is a consequence of the chosen deformation mechanism of elastic bending of fiber segments between fiber-fiber contact points. Madsen and Lilholt (2002) performed several successive compaction cycles on isotropic hemp, jute, and flax fiber assemblies and showed that the exponent almost doubled at the second compaction cycle reaching values larger than five. Further compression cycles made the exponent increase even further. It should be noted that the fiber mats used in this study are pressed before dried, as is common practice in manufacture of handsheets. Another contribution to a high exponent is fiber slippage. For lubricated mats where fibers can slip against each other, the slope in the log P-log V_f plot has been shown to become higher (Toll 1998).

In case Eq. (11) is fitted to all data points, the predicted fiber moduli become unreasonably high. This could be explained by the rather high density of the tested fiber mat, which gave an initial V_f as high as 0.26. An assumption is that the distance between the fiber-fiber contact points is large. When V_f increases the distance between the fiber-fiber contact points decreases. A key assumption of the model that the surface traction can be represented as pointwise acting forces might not be valid. Fiber length does not enter the analysis but might be important because presence of free fiber ends affects the average compliance of the deformation units, especially for low aspect ratio fibers (Toll 1998). The fibers used in this study have an aspect ratio of about 100 so that the fiber mat under self-load should form a large enough number of contact points per fiber to behave as if the fibers were infinitely long. Moreover, first-order beam theory might not be able to describe the deformation mechanism, and other theories that incorporate shear deformation should perhaps be considered. Other deformation mechanisms such as compression of the fiber wall are more likely to step in, which could also be an explanation to the stiffer behavior of the model (Jones 1963;

Provatas and Uesaka 2003; Lundquist et al. 2004). It is also probable that local deformation becomes inelastic, which ultimately leads to fiber breakage or crushing.

To exclude higher-order elastic effects from transverse fiber compression and shear stresses, the experimental data were truncated. Equation (4) was used to calculate the average of the expected number of contact points per unit length of a fiber and its inverse gave the average length of a deforming unit l (see Fig. 1b) as functions of V_f. The ratio between the mean width of the fibers $E[W]$ and the average segment length l could be used as an average measure of the 'relative bonded area' per deforming unit, denoted RBA (Sampson 2003). An approximately linear relationship between V_f and RBA was obtained. In Fig. 6 the effective Young's modulus of the fibers E_L is shown. It can be seen that the fiber stiffness is almost constant up to a critical RBA value (marked by the dashed line at the knee point in Fig. 6) where the stiffness rises drastically. The critical RBA value and the corresponding V_f value were used to truncate the experimental data. In Fig. 5, the data points marked with black squares are used to fit to Eq. (11), i.e. the black line of slope 5 in a double-logarithmic plot. The experimental data show a notably steeper slope than expected. This strain hardening effect could be attributed to straight-ening of curled fibers. The results from the other specimens were treated in the same way, and the resulting average of all tests for Young's modulus of the fibers was 20.1 GPa with a standard deviation of 1.9 GPa. It should be emphasized that this average value is merely an *effective* measure of the modulus since the exponent is higher than the expected value of five for pure beam bending. However, for fiber mats exhibiting the same deformation mechanism and same exponents, these effective values can be used as a measure of the fiber stiffness for comparison and quantification of the fiber qualities.

In a similar way the statistical data reduction steps in Eqs. (15)–(20) were applied, together with the distribution parameters of the fiber cross-sectional dimensions given in Table 1, to calculate the effective Young's modulus of the fibers. The predicted average effective modulus was 30% lower than the one estimated by brute force using Eq. (11) and the raw data from fiber cross-section measurements. The chosen lognormal distribution is limited to two parameters, μ and σ. It can be seen in Fig. 7 that even though the estimated distribution captures the main features of the empirical distribution, there is a difference in particular for the higher tail. The maximum-likelihood estimated distribution function, overestimates the occurrence probability for high values of H. This skewness manifests itself in an overestimation of $E[H^2] =$
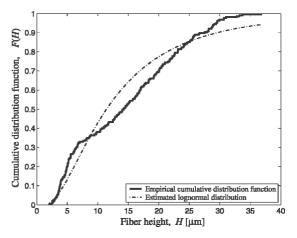

FIG. 6. The Young's modulus of the fibers, E_L vs. relative bonded area, RBA. Gray squares represent all data points, while black circles give the data up to the critical RBA value marked by the dashed line.

FIG. 7. Empirical and estimated lognormal cumulative distribution function for the fiber height H.

$E[H]^2 + \text{Var}[H]$. This is the reason for the lower effective Young's modulus after data reduction to distribution parameters as compared with the modulus value calculated directly from the entire set of sample data. Density plots revealed a tendency of a bimodal distribution of the fiber height, which indicated that the fibers are probably better categorized into two distinct early-wood and latewood fractions. There is always a trade-off between the number of distribution parameters and precision. Given the relatively large scatter of fiber dimensions, a two-parameter distribution was considered appropriate for the present data.

Tensile test results

The tensile stiffness index was determined to 9.71 (0.60) MNm/kg in the MD of the fiber mat and to 1.03 (0.16) MNm/kg in the CD. These are average values and standard deviations (given in parentheses). The volume fraction of the fibers in the fiber mat was 0.22. Before using the laminate micromechanics model, Eqs. (21)–(23), to estimate the stiffness of the fibers from the measured tensile stiffness indices, plausible values of $R_A = E_L/E_T$, and $R_S = G_{LT}/E_L$ must be established. Based on the review of literature data on the anisotropic elastic properties of wood fibers in Neagu et al. (2005) a suitable range of stiffness ratios is selected. The ratio, E_L/E_T, ranges from 2 to 10 and G_{LT}/E_L is chosen to 0.1. The major Poisson ratio is set to $\nu_{LT} = 0.3$ (Bergander and Salmén 2000). The variation of the longitudinal Young's modulus of the fibers with the anisotropy ratio, shown in Fig. 8, is not exceedingly large—from 17.4 GPa to 19.0 GPa.

The value of the longitudinal Young's modulus obtained in this study, 17.4–20.1 GPa for unbleached softwood kraft fibers, can be compared with values for similar cellulosic fibers found in literature. For fibers from Norway spruce, Scotch pine, and Douglas fir, various Young's moduli in the dry state ranging from 13 to 25 GPa have been reported, with delignified fibers and thermomechanical pulp generally
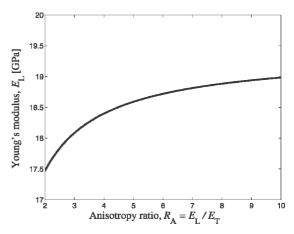

FIG. 8. The longitudinal Young's modulus of the fibers as function of the fiber anisotropy ratio for $G_{LT}/E_L = 0.1$.

having the lower values (Leopold 1966; Ehrn-rooth and Kolseth 1984).

Comparison of methods

The effective Young's modulus of the fibers of 20.1 GPa determined with the micromechanical compression model compares relatively well with the values of 17.4–19.0 GPa obtained by means of back calculation from the macroscopic elastic properties of the fiber mat. Although the methods are fundamentally different with different applicability, they provide quantitative results since the fiber volume fraction, orientation distribution, and fiber dimensional variability are taken into account. This is the main advantage with using these types of methods as the potential of various types of fibers can be investigated, even if the microstructures are different. The two methods are complementary, since the compression method is appropriate for low-density fiber mats and while the laminate model works better for high-density fiber mats.

There are some matters of concern regarding the applicability of the two methods. The compression method assumes point loads of Bernoulli-Euler beams. At high volume fractions, shear deformation and transverse fiber compression need to be taken into account. Since the fibers are elastically unbalanced due to their helical microstructure and they are fre-

quently kinked, twisting of fibers is also a likely deformation mechanism which is not modeled at this stage (Page et al. 1971). As for the tensile test of fiber mats, the laminate model assumes a dense packing of fibers and efficient stress transfer along the entire fiber lengths. The assumption of uniform strain leads to upper bounds on the elastic constants and to an overprediction of the fiber mat stiffness, thus an underestimation of the fiber Young's modulus back-calculated from fiber mat properties (Lu et al. 1995). Another source of difference between predictions and experiments can be less than perfect bonding between fibers and unbonded parts of the fibers, which are free from adjacent constraints and likely to buckle and twist on loading (Page et al. 1971; Page and Seth 1980).

The two tests are suitable at mutually exclusive microstructures. The aim of the present study was to investigate the applicability of the test methods to determine the fiber stiffness. Since fiber mats of approximately the same density were used for the two tests, it is noteworthy to see that the estimated Young's moduli of the fibers were relatively close, despite the difference in model assumptions, although the effective value from the compression test should be regarded as relatively coarse. It is probable that the investigated fiber mats have a microstructure somewhere between the two extremes, and that the estimated fiber stiffness should fall in the range between the two estimations.

Further development

It has been shown that the two alternative test-methods investigated could be adopted for the specific use in evaluation of the wood fiber stiffness. Advantages, disadvantages, and some matters of concerns regarding the present micromechanical treatment have been outlined. Some unresolved issues that remain to be addressed are discussed in this section.

To make the compression method more useful for a larger variety of wood fiber mats, further model refinements need to be done to describe the deformation mechanisms relevant for these fiber mats. A first step would be to experimen-tally identify and quantify the deformation mechanisms. This is not an easy task for the bulk of the fiber mat. A possible way would be to use X-ray microtomography for *in situ* characterization to study the change of the internal microstructure during compressive loading. This method has proven useful for static conditions in wood fiber mats (Antoine et al. 2002), as well as for tensile loading of individual wood fibers (Keckes et al. 2003). This would provide insight into fiber orientation, fiber contact density, spatial distribution of fibers, fiber bending vs. fiber compression, contact point distribution etc. In addition to fiber beam bending, the inclusion of shear deformation in the fibers and transverse fiber compression should probably also be incorporated in the model to account for the active mechanisms. This would however mean that the simplicity of the analytical formation in Eq. (11) would be lost, and a numerical approach should be necessary. A better correspondence with experimental pressure-fiber content data in Fig. 5 is anticipated in a more comprehensive model, and the estimated elastic properties of the fiber would become more trustworthy.

Another reason for studying the compressive behavior of wood fiber mats is improved understanding of manufacturing of composites. The compaction of fibrous reinforcement is common in a number of composite processing techniques. This occurs in resin transfer molding (RTM), vacuum infusion, and flow of a suspension of fibers in a viscous thermoplastic resin, e.g. hot-press molding of GMTs (Servais et al. 2001). For RTM, the degree of fiber packing controls the permeability of the fiber bed as well as necessary clamping forces to close the mold. This set the limits for achievable fiber content (Toll 1998). Since wood fibers are gaining increased use as a composite reinforcement, manufacturing issues are becoming more important.

Comparison with numerical results could also be useful. For a more precise prediction of the fiber contact density and spacing for fibers with wide distributions of cross-section dimensions, Monte Carlo simulation is an alternative. In this way, the fibers could be placed in spaces not already occupied by other fibers (Lu and Carls-

son 1996). Drawbacks are of course that many simulations must be carried out for each new material, and that the results are therefore not readily integrated into a constitutive analytical model (Alkhagen 2002). The statistical model employed here works well for dilute concentration of long fibers. For fibers with sufficiently low aspect ratios, the free fiber ends should have a significant effect on the contact density and the mean compliance of a deformation unit (Toll 1998). Finally, the assumption that distribution of incremental forces in a deformation unit is uncorrelated with its height might break down if the fibers are very different in size and stiffness.

As for the in-plane tensile test of fiber mats, it works well for high-density mats with well-bonded fibers. It would be interesting to see how it works for fiber mats with lower densities where network and hybrid or mosaic models could be more appropriate. Boundaries of the applicability of different models should be delineated. Based on a more fundamental understanding, it should be possible to develop more straightforward engineering models or rules of thumb for selection of prospective fibers for composite applications by simple testing of forms prior to composite manufacture.

CONCLUSIONS

The effective longitudinal Young's modulus of wood fibers has been determined from compaction and tensile tests of unimpregnated wood-fiber mats. A micromechanical approach was used to account for the volume fraction, orientation distribution, and dimensional variability of the fibers. In this way quantitative results can be obtained and used to evaluate the potential stiffness contribution of different types of wood fibers for reinforcement in composites. The range of applicability for the compression model is limited to low-density fiber mats of fibers with high aspect ratio. For high-density fiber mats with strong bonds and long fibers, an in-plane tensile test and a laminate model are more appropriate. The macroscopic stiffness properties of the fiber mat are then needed as input parameters. Results from the two methods

compare well despite the difference in assumptions of the two models, although the values from the compression model should be regarded as a relatively crude effective measures at this stage. Obtained values for the longitudinal Young's modulus ranged from 17.4–19 GPa (laminate model) to 20.1 GPa, (compression model) for unbleached softwood kraft fibers and are in agreement with values for similar cellulosic fibers found in literature.

REFERENCES

ALKHAGEN, M. I. 2002. Nonlinear elasticity of fiber masses. Doctoral Thesis, Department of Applied Mechanics, Chalmers University of Technology, Göteborg, Sweden.

ANTOINE, C., P. NYGÅRD, Ø. W. GREGERSEN, R. HOLMSTAD, T. WEITKAMP, AND C. RAU. 2002. 3D images of paper obtained by phase-contrast X-ray microtomography: Image quality and binarisation. Nucl. Instrum. Meth. A 490(1–2):392–402.

BERGANDER, A., AND L. SALMÉN. 2000. The transverse elastic modulus of the native wood fibre wall. J. Pulp Pap. Sci. 26(6):234–238.

BURY, K. 1998. Statistical distributions in engineering. Cambridge University Press, Cambridge, UK. 362 pp.

CICHOCKI JR., F. R., AND J. L. THOMASON. 2002. Thermoelastic anisotropy of a natural fiber. Compos. Sci. Technol. 62(5):669–678.

COX, H. L. 1952. The elasticity and strength of paper and other fibrous materials. Br. J. Appl. Phys. 3:72–79.

EHRNROOTH, E. M. L., AND P. KOLSETH. 1984. The tensile testing of single wood pulp fibers in air and in water. Wood Fiber Sci. 16(4):549–566.

FELLERS, C., H. ANDERSSON, AND H. HOLLMARK. 1986. The definition measurement of thickness and density, Pages 151–167 in J. A. Bristow, and P. Kolseth, eds. Paper Structure and Properties. Marcel Dekker, New York, NY.

GAMSTEDT, E. K., E. SJÖHOLM, C. NEAGU, F. BERTHOLD, AND M. LINDSTRÖM. 2002. Effects of fibre bleaching and earlywood-latewood fractions on tensile properties of wood-

fibre reinforced vinyl ester. Pages 185–196 *in* H. Lilholt, B. Madsen, H. L. Toftegaard, E. Cendre, M. Megnis, L. P. Mikkelsen, and B. F. Sørensen, eds. Proc. 23rd Risø International Symposium on Sustainable and Natural Polymeric Composites—Science and Technology, Risø National Laboratory, Denmark.

HAYGREEN, J. G., AND J. L. BOWYER. 1982. Forest products and wood science. The Iowa State University Press, Ames, Iowa, IA. 495 pp.

JAKLIC, A., AND F. SOLINA. 2003. Moments of superellipsoids and their application to range image registration. IEEE T. Syst. Man Cy. B 33(4):648–657.

JONES, R. L. 1963. The effect of fiber structural properties on compression response of fiber beds. TAPPI 46(1):20–28.

KAJANTO, I., J. LAAMANEN, AND M. KAINULAINEN. 1998. Paper bulk and surface, Pages 89–115 *in* K. Niskanen, ed. Paper Physics. Fapet Oy, Helsinki, Finland.

KECKES, J., I. BURGERT, K. FRUHMANN, M. MULLER, K. KOLLN, M. HAMILTON, M. BURGHAMMER, S. V. ROTH, S. STANZL-TSCHEGG, AND P. FRATZL. 2003. Cell-wall recovery after irreversible deformation of wood. Nat. Mater. 2(12):810–814.

KOMORI, T., AND K. MAKISHIMA. 1977. Number of fiber-to-fiber contacts in general fiber assemblies. Text. Res. J. 47(1):13–17.

LEOPOLD, B. 1966. Effect of pulp processing on individual fibre strength. TAPPI 49(7):315–318.

LU, W., AND L. A. CARLSSON. 1996. Micro-model of paper. Part 2: Statistical analysis of the paper structure. TAPPI 79(1):203–210.

———, ———, AND Y. ANDERSSON. 1995. Micro-model of paper. Part 1: Bounds on elastic properties. TAPPI 78(12):155–164.

———, ———, AND A. DE RUVO. 1996. Micro-model of paper. Part 3: Mosaic model. TAPPI 79(2):197–205.

LUNDQUIST, L., F. WILLI, Y. LETERRIER, AND J.-A. E. MÅNSON. 2004. Compression behavior of pulp fiber networks. Polym. Eng. Sci. 44(1):45–55.

MADSEN, B., AND H. LILHOLT. 2002. Compaction of plant fibre assemblies in relation to composite fabrication. Pages 239–250 *in* H. Lilholt, B. Madsen, H. L. Toftegaard, E. Cendre, M. Megnis, L. P. Mikkelsen, and B. F. Sørensen, eds. Proc. 23rd Risø International Symposium, Risø, Denmark.

MOSS, P. A., E. RETULAINEN, H. PAULAPURO, AND P. AALTONEN. 1993. Taking a new look at pulp and paper: Applications of confocal laser scanning microscopy (CLSM) to pulp and paper research. Pap. Puu-Pap. Tim. 75(1–2): 74–79.

NEAGU, R. C., E. K. GAMSTEDT, AND M. LINDSTRÖM. 2005. Influence of wood-fibre hygroexpansion on the dimensional instability of fibre mats and composites. Compos. Part A-Appl. S. 36(6):772–788. (In press).

NORDIN, L.-O. 2004. Wood fiber composites: From processing and structure to mechanical performance. Doctoral Thesis, Department of Applied Physics and Mechanical Engineering, Luleå University of Technology, Luleå, Sweden.

PAGE, D. H., AND R. S. SETH. 1980. The elastic modulus of paper II. The importance of fiber modulus, bonding, and fiber length. TAPPI 63(6):113–116.

———, F. EL-HOSSEINY, AND K. WINKLER. 1971. Behaviour of single wood fibres under axial tensile strain. Nature 229(5282):252–253.

———, ———, ———, AND A. P. S. LANCASTER. 1977. Elastic modulus of single wood pulp fibres. TAPPI 60(4): 114–117.

PROVATAS, N., AND T. UESAKA. 2003. Modelling paper structure and paper-press interactions. J. Pulp Pap. Sci. 29(10): 332–340.

REME, P. A., P. O. JOHNSEN, AND T. HELLE. 1999. Changes induced in early- and latewood fibres by mechanical pulp refining. Nord. Pulp Paper Res. 14(3):256–262.

SAMPSON, W. W. 2003. The statistical geometry of fractional contact area in random fibre networks. J. Pulp Pap. Sci. 29(12):412–416.

SCHULGASSER, K., AND D. H. PAGE. 1988. The influence of transverse fibre properties on the in-plane elastic behaviour of paper. Compos. Sci. Technol. 32(4):279–292.

SERVAIS, C., V. MICHAUD, AND J.-A. E. MÅNSON. 2001. The packing stress of impregnated fiber mats. Polym. Comp. 22(2):298–311.

TOLL, S. 1993. Note: On the tube model for fiber suspensions. J. Rheol. 37(1):123–125.

———. 1998. Packing mechanics of fiber reinforcement. Polym. Eng. Sci. 38(8):1337–1350.

———, AND J.-A. E. MÅNSON. 1995. Elastic compression of a fiber network. J. Appl. Mech.-T. ASME 62(1):223–226.

TSAI, S. W., AND H. T. HAHN. 1980. Introduction to Composite Materials. Technomic Publishing, Westport, CT.

UESAKA, T. 2002. Dimensional stability and environmental effects on paper properties, Pages 115–171 *in* R. E. Mark, ed. Handbook of Physical and Mechanical Testing of Paper and Paperboard. Marcel Dekker, New York, NY.

ZHU, S., H. PELTON, AND K. COLLVER. 1995. Mechanistic modelling of fluid permeation through compressible fibre beds. Chem. Eng. Sci. 50(22):3557–3572.